# Near-collapse of the geomagnetic field may have contributed to atmospheric oxygenation and animal radiation in the Ediacaran Period

Check for updates

Wentao Huang [1,2], John A. Tarduno [1,3,4,5] ✉, Tinghong Zhou [1], Mauricio Ibañez-Mejia [6], Laércio Dal Olmo-Barbosa [7], Edinei Koester[7], Eric G. Blackman [3,4], Aleksey V. Smirnov [8,9], Gabriel Ahrendt [8], Rory D. Cottrell [1], Kenneth P. Kodama [10], Richard K. Bono [11,12], David G. Sibeck[13], Yong-Xiang Li [14], Francis Nimmo [15], Shuhai Xiao [16] & Michael K. Watkeys[5]

Earth's magnetic field was in a highly unusual state when macroscopic animals of the Ediacara Fauna diversified and thrived. Any connection between these events is tantalizing but unclear. Here, we present single crystal paleointensity data from 2054 and 591 Ma pyroxenites and gabbros that define a dramatic intensity decline, from a strong Proterozoic field like that of today, to an Ediacaran value 30 times weaker. The latter is the weakest time-averaged value known to date and together with other robust paleointensity estimates indicate that Ediacaran ultra-low field strengths lasted for at least 26 million years. This interval of ultra-weak magnetic fields overlaps temporally with atmospheric and oceanic oxygenation inferred from numerous geochemical proxies. This concurrence raises the question of whether enhanced H ion loss in a reduced magnetic field contributed to the oxygenation, ultimately allowing diversification of macroscopic and mobile animals of the Ediacara Fauna.

The discovery of an ultra-low time-averaged field intensity (UL-TAFI, $0.7 \times 10^{22}$ A m$^2$) from 565 Ma anorthosites of the Sept Îles Mafic Intrusive Suite (Quebec, Canada) suggested that the geodynamo approached the weak field state where core kinetic energy exceeds magnetic energy[1,2]. Connections between unusual Ediacaran-Cambrian magnetic fields and evolutionary events[3] proposed[4] prior to report of the UL-TAFI have been challenged[5] (Supplementary Discussion—The time-averaged geomagnetic field). As emphasized by Sagan nearly 60 years earlier[6], the atmosphere and ocean can shield life from energetic solar particles. For atmospheric loss

controlled by the magnetosphere[7] to have played an important role, it must have acted over a relatively long time interval, and/or involved processes amplifying escape, overcoming bounds imposed by the slow upward diffusion of atmospheric constituents[8].

The Sept Îles UL-TAFI record is supported by paleointensity investigations of Ediacaran lavas and dikes[9]. Nevertheless the data have limitations. Thellier analyses of samples dominated by single domain magnetic carriers are the gold standard for paleointensity determination because only these data are solidly based on thermoremanent magnetization theory[10].

[1]Department of Earth and Environmental Sciences, University of Rochester, Rochester, NY 14627, USA. [2]State Key Laboratory of Tibetan Plateau Earth System, Environment and Resources (TPESER), Institute of Tibetan Plateau Research, Chinese Academy of Sciences, 100101 Beijing, China. [3]Department of Physics & Astronomy, University of Rochester, Rochester, NY 14627, USA. [4]Laboratory for Laser Energetics, University of Rochester, Rochester, NY 14623, USA. [5]Geological Sciences, University of KwaZulu-Natal, Durban 4000, South Africa. [6]Department of Geosciences, University of Arizona, Tucson, AZ 85721, USA. [7]Instituto de Geociências, Universidade Federal do Rio Grande do Sul, Porto Alegre, RS, Brazil. [8]Department of Geological and Mining Engineering and Sciences, Michigan Technological University, Houghton, MI 49931, USA. [9]Department of Physics, Michigan Technological University, Houghton, MI 49931, USA. [10]Department of Earth and Environmental Sciences, Lehigh University, Bethlehem, PA 18015, USA. [11]Department of Earth, Ocean and Atmospheric Science, Florida State University, Tallahassee, FL 32306, USA. [12]Geomagnetism Laboratory, University of Liverpool, Liverpool L69 3GP, UK. [13]Code 670, NASA/Goddard Space Flight Center, Greenbelt, MD 20771, USA. [14]State Key Laboratory for Mineral Deposits Research, Institute of Continental Geodynamics, School of Earth Science and Engineering, Nanjing University, Nanjing 210046, China. [15]Department of Earth and Planetary Sciences, University of California, Santa Cruz, CA 95064, USA. [16]Department of Geosciences, Virginia Tech, Blacksburg, VA 24061, USA. ✉e-mail: john@earth.rochester.edu

Moreover, because the geomagnetic field exhibits short term secular variation, time-averaging is needed to detect trends reflecting evolving core processes (Supplementary Discussion—The time-averaged geomagnetic field). The Sept Îles Thellier data are time-averaged (~75 kyr) by virtue of the slow cooling of the anorthosites studied[1]. But this key time-averaged aspect has not yet been replicated with Thellier data from single domain dominated samples of other localities.

Bono et al.[1] used single crystal paleointensity (SCP)[11] analyses to isolate ideal magnetic records. The feldspar and pyroxene crystals measured contained magnetic needles exsolved along crystallographic planes[12]. Scanning electron microscopy (SEM) analyses and magnetic hysteresis data confirmed their SD nature. Herein, we examine both the accuracy and duration the UL-TAFI through a comparison of SCP analyses of 2054 Ma (South Africa)[13] and 591 Ma (Brazil)[14] rocks that come from a layered mafic intrusion and post-collisional magmatic suite, respectively, where prior paleomagnetic and geochronological studies have demonstrated the preservation of primary magnetizations (Supplementary Discussion—Geologic context and prior work). Plagioclase from the rocks studied have single domain magnetic characteristics nearly identical to those of the Sept Îles samples studied by Bono et al.[1]. Motivated by the results, we then examine anew the potential connections of the geomagnetic field and Ediacaran to Cambrian evolution, and propose linkages with the paleomagnetosphere[15,16] and oxygenation[17–20].

## Results

We collected eight plagioclase-bearing pyroxenite hand samples in the 2054 ± 1.3 Ma[13] Rustenberg Layered Intrusion of the Bushveld Complex in northern South Africa (Supplementary Fig. 1a; "Materials and methods"). Magnetic susceptibility versus temperature curves (K-T; Supplementary Fig. 2a, b; "Materials and methods") indicate that Ti-poor titanomagnetite and pure magnetite are the dominant magnetic carriers in bulk samples (Supplementary Discussion—Rock magnetism of whole rocks). Magnetic hysteresis loops ("Materials and methods") of small bulk-rock specimens (Supplementary Fig. 2c, d) have relatively low coercive force ($\overline{B_c}$ = 13.6 ± 8.5 mT), remanent coercivity ($\overline{B_{cr}}$ = 60.8 ± 31.2 mT), and squareness ($\overline{M_{rs}/M_s}$ = 0.16 ± 0.09; Supplementary Table 1). These data suggest the presence of pseudosingle domain and multidomain magnetic grains (Supplementary Fig. 3a). In contrast, selected optically clear plagioclase grains have wide, open hysteresis loops (Fig. 1a and Supplementary Fig. 2e, f) and high values ($\overline{B_c}$ = 69.1 ± 15.7 mT, $\overline{B_{cr}}$ = 107.5 ± 19.7 mT, $\overline{M_{rs}/M_s}$ = 0.48 ± 0.08) (Supplementary Table 1), indicating the presence of single domain grains (Supplementary Fig. 3a).

The extraordinary magnetic recording properties of the plagioclase crystals are further supported by first order reversal curve (FORC) analysis and SEM analyses ("Materials and methods"). FORC diagrams of all clean plagioclase specimens are highly peaked on the $B_u = 0$ axis and the contours are elongated with negligible vertical spread (Fig. 1b and Supplementary Fig. 4), indicating the presence of noninteracting single domain grains. SEM and energy-dispersive X-ray spectroscopy (EDS) data reveal that iron-titanium oxide needles are omnipresent (Fig. 1c, d). The width of the needles is <500 nm, and the length varies widely, but is often several μm. The presence of Ti further implicates a high temperature of formation[12], indicating that the needles can carry a primary thermoremanent magnetization.

We investigated absolute paleointensity by SCP Thellier-Coe analyses utilizing $CO_2$ laser heating[21] with partial thermal remanent magnetization (pTRM) checks and selection criteria following prior SCP studies[1,22] (Fig. 1e, f and Supplementary Fig. 5, "Materials and methods"). Twenty-two of the 175 crystals measured met selection criteria (17 are category A samples, and 5 are category B samples; Supplementary Table 2). The main cause of rejection was failed pTRM checks. The characteristic remanent magnetization used for paleointensity calculation was isolated between 360 and 580 °C. A single crystal from one hand sample (BQ1-D.14) showed higher unblocking, to 620 °C (Supplementary Fig. 5g and Supplementary Table 2). Categories A and B samples with applied field of 30 μT yield a mean paleointensity of 67.4 ± 3.7 μT ($n = 13$), and samples with applied

field of 60 μT (all category A) define a mean paleointensity of 71.2 ± 4.6 μT ($n = 9$). These mean values appear to be drawn from the same population (Supplementary Discussion—Applied field bias and recording replication, Supplementary Fig. 6), suggesting no correlation with the strength of the applied TRM[23]. The average paleointensity from all category A and B samples is 69.0 ± 4.3 μT ($n = 22$). We correct for cooling rate using a factor of 1.5 (Supplementary Discussion—Paleointensity corrections (cooling rate and anisotropy) which yields a paleointensity of 48.6 ± 3.0 μT ($n = 22$); we further apply anisotropy corrections ("Materials and methods"; Supplementary Discussion—Paleointensity corrections (cooling rate and anisotropy) leading to a paleointensity estimate of 49.1 ± 2.4 μT (Supplementary Table 3). Using a paleolatitude[24] of 45°N (Supplementary Discussion—Geologic context and prior work) a paleomagnetic dipole moment of $8.04 ± 0.40 × 10^{22}$ A m$^2$ is calculated.

The Passo da Fabiana Gabbros occur as intrusions in the Dom Feliciano Belt of southern Brazil[14]. Here we focus on a sample previously studied for geochronology[14] ("Materials and methods", Supplementary Fig. 1b, c) for single crystal paleointensity analysis. Sample GPF-01 is a coarse-grained gabbro; U-Pb SHRIMP age data on zircons from sample GPF-01 yield an age[14] of 591.2 ± 3.5 Ma. We also investigated another gabbro (sample GPF-110) from the same unit but collected from an outcrop ~1 km away for replication. K-T curves for GPF-01 whole rock samples show the dominant presence of magnetite, along with a FeTi phase (Supplementary Fig. 7a). For GPF-110, these data indicate magnetite, but also a change near 320 °C characteristic of pyrrhotite[10] (Supplementary Fig. 7b). Magnetic hysteresis data for groundmass samples of both GPF-01 and GPF-110 show narrow loops reflecting relatively low coercive force, remanent coercivity and squareness ($\overline{B_c}$ = 8.2 ± 4.1 mT, $\overline{B_{cr}}$ = 23.1 ± 7.4 mT, $\overline{M_{rs}/M_s}$ = 0.13 ± 0.08; Supplementary Table 4 and Supplementary Fig. 7c, d), consistent with pseudosingle domain and multidomain carriers, whereas curves for clean feldspars from these rocks define broad open loops ($\overline{B_c}$ = 52.8 ± 6.6 mT, $\overline{B_{cr}}$ = 92.3 ± 3.8 mT, $\overline{M_{rs}/M_s}$ = 0.43 ± 0.06) indicating single domain carriers (Fig. 2a and Supplementary Figs. 3b and 7e, f). FORC diagrams for single crystals show a narrow central ridge ($B_u = 0$) typical of single domain grains (Fig. 2b and Supplementary Fig. 8). SEM and EDS analyses define the presence of needle-like magnetic inclusions, ≤200 nm in width with variable lengths up to several μm, with varying Fe and Ti content (Fig. 2c, d). No SEM/EDS evidence for pyrrhotite is found in the feldspar samples we analyzed.

Initial SCP Thellier-Coe experiments with laser heating[11,21] indicated remanent fields only a fraction as strong as those preserved by the Bushveld plagioclase crystals, leading us to use lower applied fields (30, 15 and 7.5 μT). Measurement of 29 crystals yielded 21 acceptable results (17 Type A, 4 Type B) with ChRMs and paleointensities isolated between 366 and 548 °C (Fig. 2e, f; Supplementary Fig. 9 and Supplementary Table 5). Most results are from GPF-01, but 3 crystals from GPF-110 give comparable values (Supplementary Discussion—Applied field bias and recording replication, Supplementary Fig. 10). The combined paleointensities obtained are 3.43 ± 0.73, 2.31 ± 0.40 and 2.72 ± 0.60 μT for 30, 15 and 7.5 μT applied fields, respectively. While there is no clear progression in the data, the mean of the value determined using a 30 μT field is higher than that obtained at lower fields, hinting at an applied field bias[23]. The average paleointensity from all these categories A and B samples using all applied field is 2.73 ± 0.69 μT ($n = 21$). We use a factor of 1.5 as a cooling rate correction (Supplementary Discussion—Paleointensity corrections (cooling rate and anisotropy), yielding an average paleointensity of 1.82 ± 0.46 μT ($n = 21$).

Anisotropy measurements and subsequent corrections reveal more clearly that paleointensity values obtained at 30 μT are higher than those obtained using lower applied fields (Supplementary Table 6). Accordingly, we select paleointensity and anisotropy data only from those experiments using applied fields of 15 and 7.5 μT. Applying both the cooling rate correction and anisotropy corrections (Supplementary Table 6) yields a paleointensity of 1.49 ± 0.10 μT. Using a paleolatitude of 42.2°S based on a pole position from the Sierra de las Ánimas complex (Uruguay)[25]
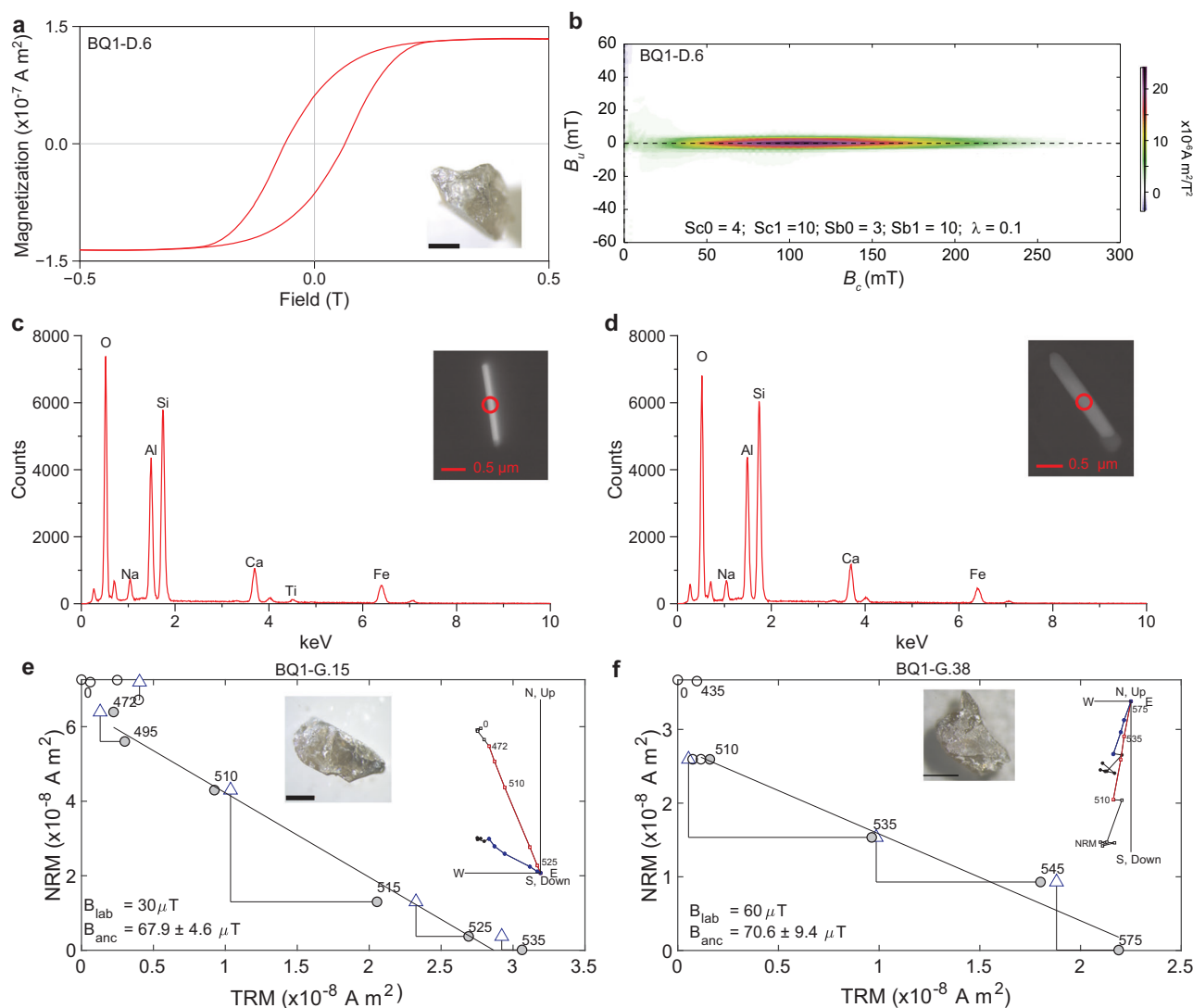
**Fig. 1 | Rock magnetic, SEM, and paleointensity analysis of plagioclase crystals from Bushveld pyroxenites. a** Magnetic hysteresis loop with images of the measured plagioclase crystal (lower right, scale bar 1 mm). **b** First order reversal curve (FORC) diagram for plagioclase crystal. **c, d** Backscatter SEM images of elongated magnetic inclusions observed in the plagioclase crystals (inset) and their corresponding EDS spectra in 20 keV. EDS spots analyzed are marked as red circles in the inset images. **e, f** NRM lost versus TRM gained (circles) and pTRM checks (triangles). All labeled points are °C. Gray circles are steps used in fit (applied field $B_{lab}$ and paleointensity value $B_{anc}$ shown in lower left). Insets: crystal measured shown in top center with 1 mm scale bar. Orthogonal vector plot of field-off steps is shown in upper right. Squares are vertical projection of the magnetization; circles are horizontal projection. Temperature ranges used in the paleointensity fit shown in color.

(Supplementary Discussion—Geologic context and prior work) the paleomagnetic dipole moment is $0.25 \pm 0.02 \times 10^{22}$ A m$^2$.

## Discussion

The plagioclase studied from the Bushveld pyroxenite and Passo da Fabiana Gabbros have ideal single domain magnetic behavior yet yield vastly different field strengths. The Bushveld value extends the Archean period of high time-averaged field intensity into the Paleoproterozoic (Fig. 3). In stark contrast, the Passo da Fabiana value is 30 times weaker, and the lowest time-averaged field strength known to date (Fig. 3a, b). When combined with the Sept Îles 565 Ma paleomagnetic dipole moment[1], the data suggests the UL-TAFI (defined as fields equal to or less than 10% of the present-day) spanned at least 26 million years. If the UL-TAFI is the nadir of the proposed much longer-term decline of field strength preceding the onset of inner core nucleation[1,22] (Supplementary Discussion—Long-term paleointensity history and ICN, Fig. 3), the duration of low (defined here as equal to or less than 20% of the present-day) to ultra-low fields could have been >200 m.y.

The new data confirming and extending the UL-TAFI strengthen a potential linkage with the Ediacaran evolution of macroscopic animals.

While phylogenomic data indicate that the animal kingdom and many phyla may have diverged prior to the Ediacaran Period[26,27], paleontological data show that the diversification of macroscopic animals, as archived in the Avalon and White Sea assemblages of the Ediacara Fauna, began at ~575 Ma and reached a climax at ~565 Ma[28–32], in a striking temporal correlation with the UL-TAFI (Fig. 3b). Prior explanations for the appearance of the Ediacara Fauna and the Cambrian radiation have centered on genetic, ecological, or environmental driving factors[33]. The temporal coincidence between the UL-TAFI and the rise of the Ediacara Fauna, however, invites a refocus on environmental factors, particularly atmospheric and oceanic oxygenation events.

Oxygen has long been identified as a key "environmental gatekeeper"[34], allowing for evolutionary innovation and for meeting the energy demands of animals[35]. Although sponges and microscopic animals can survive at low levels of dissolved oxygen (as low as ~1.5 μM, equivalent to 0.5% present atmospheric level [PAL][36,37]), macroscopic, morphologically complex, and mobile animals require a greater amount of oxygen to support their metabolic demands[38]. A complex animal ecosystem involving long food chains and predators requires still greater amounts of oxygen, as indicated by the
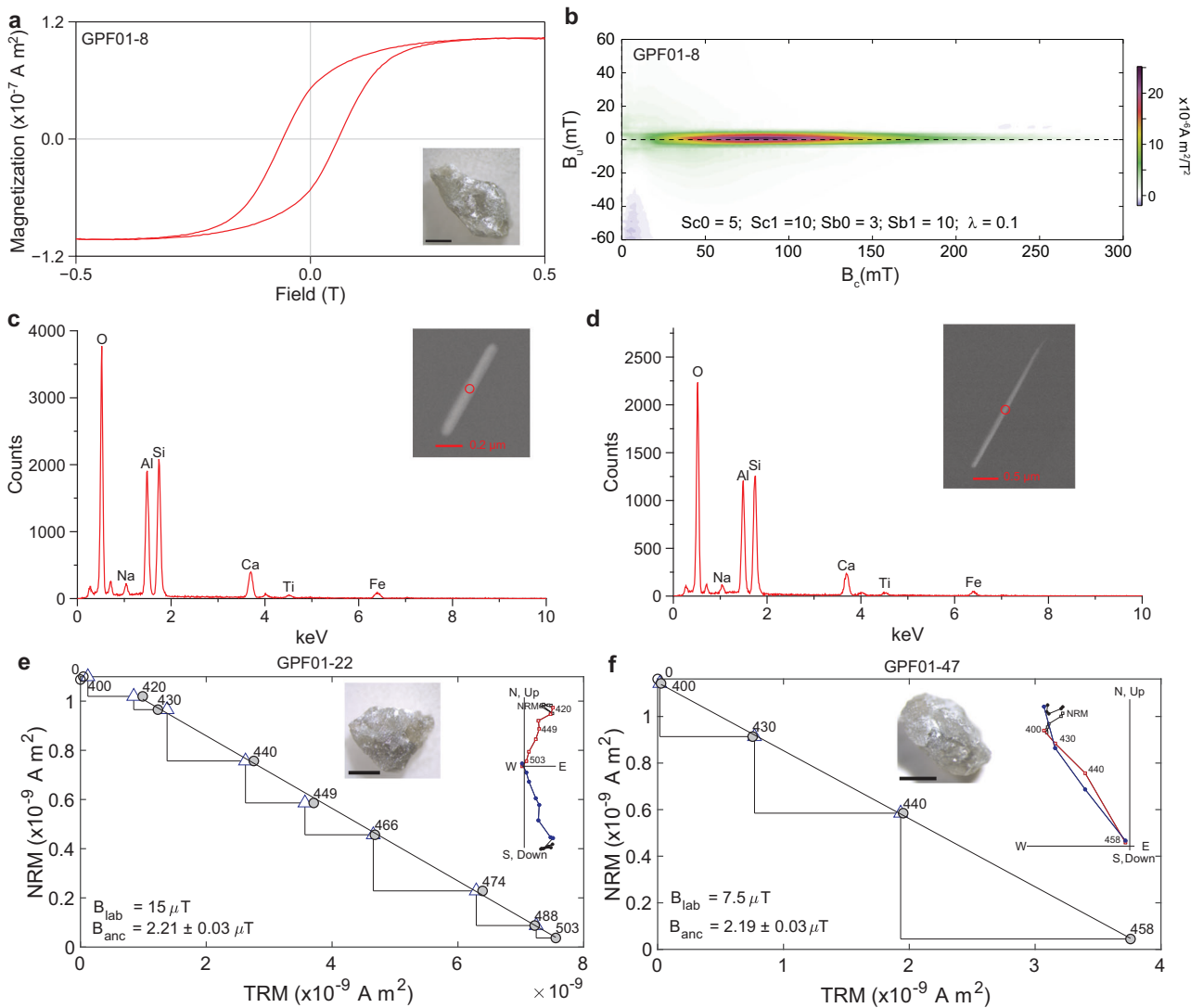
**Fig. 2 | Rock magnetic, SEM, and paleointensity analysis of plagioclase crystals from the Passo da Fabiana Gabbros. a** Magnetic hysteresis loop with images of the measured plagioclase crystal (lower right, scale bar 1 mm). **b** First order reversal curve (FORC) diagram for plagioclase crystal. **c, d** Backscatter SEM images of elongated magnetic inclusions observed in the plagioclase crystals (inset) and their corresponding EDS spectra in 20 keV. EDS spots analyzed are marked as red circles in the inset images. **e, f** NRM lost versus TRM gained (circles) and pTRM checks (triangles). All labeled points are °C. Gray circles are steps used in fit (applied field $B_{lab}$ and paleointensity value $B_{anc}$ shown in lower left). Insets: crystal measured shown in top center with 1 mm scale bar. Orthogonal vector plot of field-off steps is shown in upper right. Squares are vertical projection of the magnetization; circles are horizontal projection. Temperature ranges used in the paleointensity fit are shown in color.

exclusion of such complex ecosystems from the modern oxygen minimum zone[39], which is characterized by dissolved $O_2$ levels of <20–30 μM or <10% PAL. In this regard, it is important to note that mobile animals and macroscopic animals up to decimeters in size have been recorded in the ~565 Ma White Sea assemblage of the Ediacara biota[40,41].

Multiple lines of geochemical evidence point to a possible increase in atmospheric and oceanic $O_2$ levels in the late Ediacaran Period, specifically in the period of ~575–565 Ma characterized by negative $\delta^{13}C$ values of the Shuram excursion[42] (Fig. 3b). These include elevated $\delta^{88}Mo$ and $\delta^{82/76}Se$ values, as well as [Mo], [U], and [V] concentrations in organic-rich shales deposited approximately at $565 \pm 5$ Ma and thus coincident with the diversification of macroscopic animals in the White Sea assemblage of the Ediacara biota[20,43]. Importantly, $\delta^{238}U$ data of carbonate rocks, as well as $\Delta'^{17}O$-$\delta^{34}S$-$\delta^{18}O$ of carbonate-associated sulfate, point to multimillion years of oceanic oxygenation that temporally coincide with the Shuram excursion and the Avalon-White Sea assemblages[44–46]. We note that there is much uncertainty and controversy with the regard of the magnitude of this oxygenation event[47,48], partly because different geochemical proxies have

different sensitivities and hence sometimes give apparently conflicting inferences about oxygen levels. Such uncertainty is further complicated by the dynamic nature of oceanic redox history and spatial heterogeneity of oceanic redox conditions in the late Ediacaran Period[49–51]. However, the concurrence of these independent indicators of oxygenation, paleontological records documenting the rise of the Ediacara Fauna, and paleomagnetic data defining the UL-TAFI merits further exploration for potential linkages.

Hydrogen (H) can escape to space by thermal and non-thermal mechanisms resulting in net oxygenation of the atmosphere[52]. Changes in climate and/or methane release recorded by Ediacaran isotopic records, including the Shuram excursion[42,53] (Fig. 3b), could have led to conditions favoring H loss, but these interpretations are debated[54] (Supplementary Discussion—Oxygenation, Ediacaran climate and methane). Here we focus on the potential influence of the UL-TAFI on H loss through changes in the paleomagnetosphere.

Using solar wind evolution models based on solar analogs[15], steady-state magnetopause stand-off distances would have been <4.5 Earth radii

**Fig. 3 | Paleointensity, oxygen and animal evolution. a** Field strength constrained from select Thellier (thermal) SCP studies (blue squares, hexagons) and bulk rock studies (gray squares) updated from Zhou et al.[22], with new time-averaged SCP results (red hexagons) reported here. Large squares are time-averaged paleomagnetic dipole moments; small squares are virtual dipole moments (VDMs). Gray circles are select Phanerozoic VDMs from Bono et al.[1]. Field evolution model (3450 Ma to 565 Ma, red line) is weighted second-order polynomial regression of Precambrian field strength data from Bono et al.[1]; 565 to 532 Ma trend from Zhou et al.[22]. **b** Cryogenian to Cambrian field strength evolution corresponding to dashed rectangle in (**a**). Open circles are results from non-Thellier methods (non-thermal and thermal) and their sizes are weighted by the numbers of cooling units from Zhou et al.[22]. Key: green, microwave method; purple, Shaw method; black, Wilson method. Brown open circles are Thellier thermal results. Ultra-low time averaged field interval (UL-TAFI) highlighted by light purple rectangle. Also shown are selenium isotopic data (open symbols) and oxygenation interpretation from Pogge von Strandmann et al.[20] (shown here with a 25 my window mean and $1\sigma$ error), summary animal radiation of bilaterian and non-bilaterians from Zhuravlev and Wood[65]), Wood et al.[3], Darroch et al.[66] and Muscente et al.[67], and Shuram excursion ages from Rooney et al.[42].
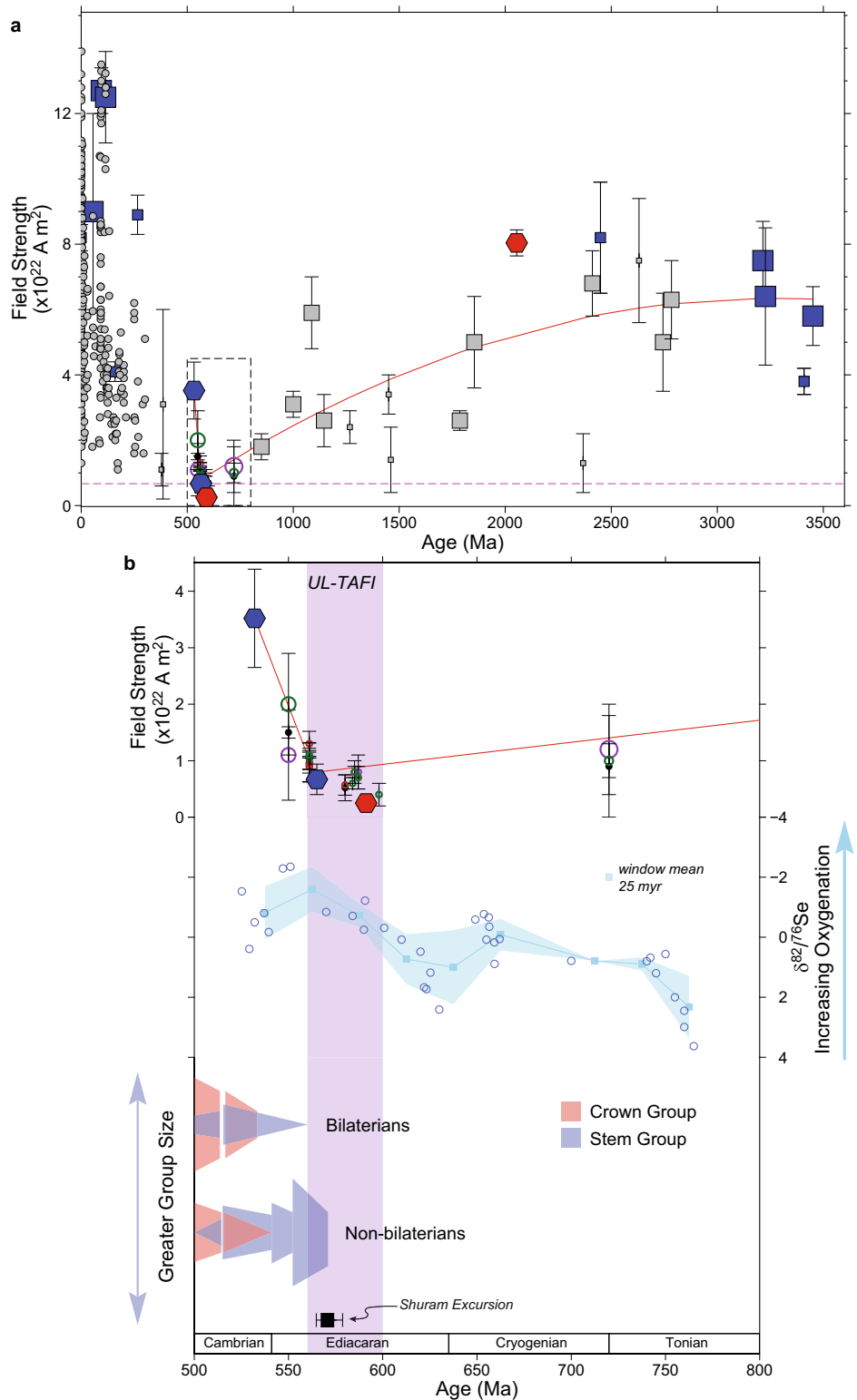


($r_\oplus$) at 565 Ma[1] and <4.2$r_\oplus$ at 591 Ma, compared to the present-day value of ~10.7$r_\oplus$. During extreme coronal mass ejection events, stand-off distances could have been as low as 1.6$r_\oplus$. These smaller standoff distances can lead to more hydrogen escape because they increase the polar cap area of open field lines[16] where non-thermal H$^+$ loss occurs today. The steady-state polar cap area of open field lines would have been 3.5 times greater at 591 Ma, and

even greater during coronal mass ejection events impacting Earth (Supplementary Discussion—Magnetopause standoff, hydrogen loss and hydrogen supply). Moreover, at the reduced stand-off distances implied by our data, the magnetopause will approach, and even fall below Earth's plasmapause[16,55], below which plasma density, dominated by H$^+$, markedly increases (Supplementary Discussion—Magnetopause standoff, hydrogen

**Article**

loss and hydrogen supply). In this case, increased global loss of $H^+$ is expected. Greater global non-thermal H loss is also predicted for the much smaller magnetosphere resulting from the UL-TAFI because the solar wind has greater access to a higher density of H atoms (Supplementary Discussion—Magnetopause standoff, hydrogen loss and hydrogen supply).

Quantifying H loss for Earth with an ultra-low field is challenging as it is observationally inaccessible. The few available models predict greater H loss[56], but the predicted change vary depending on assumptions (~30% to 10 times). The highest estimates could result in a few percent change of oxygen (PAL) that might represent a perturbation or crossing of a threshold, allowing Ediacaran animal diversification (Supplementary Discussion—Magnetopause standoff, hydrogen loss and hydrogen supply), but it should be noted that none of these nascent models consider all of the processes discussed above.

An effect that also warrants further consideration is that with decreased magnetopause standoff, greater penetration of highly energetic protons is expected over a larger solid angle, resulting in the formation of $NO_x$ compounds which can create ozone holes[57]. With the greater UV flux (Supplementary Discussion—Magnetopause standoff, hydrogen loss and hydrogen supply), dissociation of water vapor[58] is expected, increasing the supply of H moving upward. Thus, the UL-TAFI could have led to both an increased supply of H available for loss, and an increased outflow.

Enhanced H loss from the magnetosphere could have acted over tens or hundreds of millions of years when the geomagnetic field was at low to ultra-low strengths (Fig. 3). The multiple pathways discussed above provide a framework for future studies quantifying hydrogen loss, oxygenation of the atmosphere and the potential consequences on the evolution of complex animals highlighted by the synchroneity of these phenomena and the near collapse of the geodynamo.

## Materials and methods

Samples were collected from the Rustenberg Layered Intrusion of the Bushveld Complex, South Africa, at 25° 33.812' S, 27° 32.480' E and from the Passo da Fabiana Gabbros at 31° 38.391' S, 53° 22.172' W (GPF-01) and 31° 37.893' S, 53° 21.815' W (GPF-110). The Rustenberg samples were collected as unoriented hand samples from a quarry exposure ensuring the study of fresh material, whereas the Passo da Fabiana samples are unoriented splits of larger samples used in prior petrological, geochemical and geochronological studies[14] ensuring both the study of fresh material and an exact correspondence of age constraints. Rock preparation, rock magnetic and paleointensity analyses were done in the paleomagnetic laboratories at the University of Rochester, and supplemented with select magnetic susceptibility measurements of Passo da Fabiana samples at Michigan Tech. Unoriented single plagioclase crystals were picked by hand from rock crushes. Grains selected for magnetic hysteresis and paleointensity measurements are free of visible inclusions when viewed under ×10 magnification. We used a Geofyzika KLY-4C KappaBridge for the bulk-rock magnetic susceptibility measurements in air at the University of Rochester and a AGICO MFK1-FA (in air) at Michigan Tech. A Princeton Measurements Corporation Alternating Gradient Force Magnetometer was used for magnetic hysteresis measurements. First order reversal curves data[59] were processed by FORCinel and VARIFORC software[60,61]. SEM observation and energy-dispersive X-ray spectroscopy analyses used a Zeiss Auriga Scanning Electron Microscope, in the Integrated Nanosystems Center at the University of Rochester.

Plagioclase grains selected for paleointensity analyses have NRM moments greater than $1 \times 10^{-10}$ A m². For the Thellier-Coe paleointensity experiments, samples were mounted on quartz holders having moments $\leq 1 \times 10^{-12}$ A m², and measured using a 2G Enterprises 755 3-component DC SQUID magnetometer with high resolution sensing coils housed in a magnetically shielded room with ambient field <200 nT at the University of Rochester. The non-magnetic purity of mounting material (sodium silicate) has been confirmed by SQUID microscope analyses[62]. Samples were heated using Synrad v20 and v40 $CO_2$ lasers calibrated using optical pyrometers[63].

Paleointensity selection criteria are as follows: Category A samples, (1) the natural remanent magnetization (NRM) versus TRM slope must include at least four steps; (2) the $R^2$ of the NRM/TRM slope fit must be greater than 0.9; (3) the field-off NRM values must trend to the origin of the orthogonal vector plots with a maximum angular dispersion ≤10°; and (4) at least three temperature steps of pTRM checks must be included and the values must be within 15%. Category B samples meet Category A criteria with only one criterion relaxed (Supplementary Tables 2 and 5).

Measurement of TRM anisotropy[64] follow the procedures described in Bono et al.[1]. The sample was first heated to an intermediate unblocking temperature without an applied field. Next, the sample was heated to the same temperature step in a 7.5, 15, 30 or 60 µT magnetic field along six orthogonal axes (+Z, −Z, +X, −X, +Y, and −Y). The magnetization of the sample was measured after each field-on heating. A multidomain tail check was performed after the six field-on steps to test for alteration.

## Data availability

Magnetic datasets generated during and/or analyzed in this study are available in the MagIC repository, http://earthref.org/MagIC/19610. Original data published in this manuscript is available at https://doi.org/10.6084/m9.figshare.25343248.

## References

1. Bono, R. K., Tarduno, J. A., Nimmo, F. & Cottrell, R. D. Young inner core inferred from Ediacaran ultra-low geomagnetic field intensity. *Nat. Geosci.* **12**, 143–147 (2019).
2. Driscoll, P. E. Simulating 2 Ga of geodynamo history. *Geophys. Res. Lett.* **43**, 5680–5687 (2016).
3. Wood, R. et al. Integrated records of environmental change and evolution challenge the Cambrian Explosion. *Nat. Ecol. Evol.* **3**, 528–538 (2019).
4. Meert, J. G., Levashova, N. M., Bazhenov, M. L. & Landing, E. Rapid changes of magnetic field polarity in the late Ediacaran: linking the Cambrian evolutionary radiation and increased UV-B radiation. *Gondwana Res.* **34**, 149–157 (2016).
5. Lingam, M. Revisiting the biological ramifications of variations in Earth's magnetic field. *Astrophys. J. Lett.* **874**, L28 (2019).
6. Sagan, C. Is the early evolution of life related to the development of the Earth's core? *Nature* **206**, 448–448 (1965).
7. Blackman, E. G. & Tarduno, J. A. Mass, energy, and momentum capture from stellar winds by magnetized and unmagnetized planets: implications for atmospheric erosion and habitability. *Mon. Not. R. Astron. Soc.* **481**, 5146–5155 (2018).
8. Hunten, D. Escape of light gases from planetary atmospheres. *J. Atmos. Sci.* **30**, 1481–1494 (1973).
9. Shcherbakova, V. et al. Ultra-low palaeointensities from East European Craton, Ukraine support a globally anomalous palaeomagnetic field in the Ediacaran. *Geophys. J. Int.* **220**, 1928–1946 (2020).
10. Dunlop, D. J. & Özdemir, Ö. *Rock Magnetism: Fundamentals and Frontiers*, Vol. 3 (Cambridge University Press, 1997).
11. Tarduno, J. A., Cottrell, R. D. & Smirnov, A. V. The paleomagnetism of single silicate crystals: recording geomagnetic field strength during mixed polarity intervals, superchrons, and inner core growth. *Rev. Geophys.* **44**, RG1002 (2006).
12. Feinberg, J. M., Scott, G. R., Renne, P. R. & Wenk, H.-R. Exsolved magnetite inclusions in silicates: features determining their remanence behavior. *Geology* **33**, 513–516 (2005).
13. Scoates, J. S. & Friedman, R. M. Precise age of the platiniferous Merensky Reef, Bushveld Complex, South Africa, by the U-Pb zircon chemical abrasion ID-TIMS technique. *Econ. Geol.* **103**, 465–471 (2008).

14. Dal Olmo-Barbosa, L., Koester, E., Vieira, D. T., Porcher, C. C. & Cedeño, D. G. Crystallization ages of the basic intrusive Ediacaran magmatism in the southeastern Dom Feliciano Belt, southernmost Brazil: implications in the belt geodynamic evolution. *J. South Am. Earth Sci.* **108**, 103143 (2021).

15. Tarduno, J. A. et al. Geodynamo, solar wind, and magnetopause 3.4 to 3.45 billion years ago. *Science* **327**, 1238–1240 (2010).

16. Siscoe, G. & Chen, C. Paleomagnetosphere. *J. Geophys. Res. Space Phys.* **80**, 4675–4680 (1975).

17. Canfield, D. E., Poulton, S. W. & Narbonne, G. M. Late-Neoproterozoic deep-ocean oxygenation and the rise of animal life. *Science* **315**, 92–95 (2007).

18. Scott, C. et al. Tracing the stepwise oxygenation of the Proterozoic ocean. *Nature* **452**, 456–459 (2008).

19. Partin, C. A. et al. Large-scale fluctuations in Precambrian atmospheric and oceanic oxygen levels from the record of U in shales. *Earth Planet. Sci. Lett.* **369-370**, 284–293 (2013).

20. Pogge von Strandmann, P. A. E. et al. Selenium isotope evidence for progressive oxidation of the Neoproterozoic biosphere. *Nat. Commun.* **6**, 10157 (2015).

21. Tarduno, J. A., Cottrell, R. D., Watkeys, M. K. & Bauch, D. Geomagnetic field strength 3.2 billion years ago recorded by single silicate crystals. *Nature* **446**, 657–660 (2007).

22. Zhou, T. et al. Early Cambrian renewal of the geodynamo and the origin of inner core structure. *Nat. Commun.* **13**, 4161 (2022).

23. Selkin, P. A., Gee, J. S. & Tauxe, L. Nonlinear thermoremanence acquisition and implications for paleointensity data. *Earth Planet. Sci. Lett.* **256**, 81–89 (2007).

24. Letts, S., Torsvik, T. H., Webb, S. J. & Ashwal, L. D. Palaeomagnetism of the 2054 Ma Bushveld Complex (South Africa): implications for emplacement and cooling. *Geophys. J. Int.* **179**, 850–872 (2009).

25. Rapalini, A. E. et al. The late Neoproterozoic Sierra de las Animas Magmatic Complex and Playa Hermosa Formation, southern Uruguay, revisited: paleogeographic implications of new paleomagnetic and precise geochronologic data. *Precambrian Res.* **259**, 143–155 (2015).

26. Erwin, D. H. et al. The Cambrian conundrum: early divergence and later ecological success in the early history of animals. *Science* **334**, 1091–1097 (2011).

27. Dohrmann, M. & Woerheide, G. Dating early animal evolution using phylogenomic data. *Sci. Rep.* **7**, 3599 (2017).

28. Narbonne, G. M. The Ediacara biota: neoproterozoic origin of animals and their ecosystems. *Annu. Rev. Earth Planet. Sci.* **33**, 421–442 (2005).

29. Shen, B., Dong, L., Xiao, S. & Kowalewski, M. The Avalon explosion: evolution of Ediacara morphospace. *Science* **319**, 81–84 (2008).

30. Xiao, S. & Laflamme, M. On the eve of animal radiation: phylogeny, ecology and evolution of the Ediacara biota. *Trends Ecol. Evol.* **24**, 31–40 (2009).

31. Droser, M. L., Tarhan, L. G. & Gehling, J. G. The rise of animals in a changing environment: global ecological innovation in the Late Ediacaran. *Annu. Rev. Earth Planet. Sci.* **45**, 593–617 (2017).

32. Matthews, J. J. et al. A chronostratigraphic framework for the rise of the Ediacaran macrobiota: new constraints from mistaken point ecological reserve, Newfoundland. *GSA Bull.* **133**, 612–624 (2020).

33. Knoll, A. H. & Carroll, S. B. Early animal evolution: emerging views from comparative biology and geology. *Science* **284**, 2129–2137 (1999).

34. Cloud Jr, P. E. Atmospheric and hydrospheric evolution on the primitive earth: both secular accretion and biological and geochemical processes have affected Earth's volatile envelope. *Science* **160**, 729–736 (1968).

35. Payne, J. L. et al. The evolutionary consequences of oxygenic photosynthesis: a body size perspective. *Photosynth. Res.* **107**, 37–57 (2011).

36. Sperling, E. A., Halverson, G. P., Knoll, A. H., Macdonald, F. A. & Johnston, D. T. A basin redox transect at the dawn of animal life. *Earth Planet. Sci. Lett.* **371–372**, 143–155 (2013).

37. Mills, D. B. et al. Oxygen requirements of the earliest animals. *Proc. Natl Acad. Sci.* **111**, 4168–4172 (2014).

38. Xiao, S. 6.10—Oxygen and early animal evolution. in *Treatise on Geochemistry* 2nd edn (eds Holland, H. D. & Turekian, K. K.) 231–250 (Elsevier, 2014).

39. Sperling, E. A. et al. Oxygen, ecology, and the Cambrian radiation of animals. *Proc. Natl Acad. Sci.* **110**, 13446–13451 (2013).

40. Evans, S. D., Gehling, J. G. & Droser, M. L. Slime travelers: early evidence of animal mobility and feeding in an organic mat world. *Geobiology* **17**, 490–509 (2019).

41. Ivantsov, A., Nagovitsyn, A. & Zakrevskaya, M. Traces of locomotion of Ediacaran macroorganisms. *Geosciences* **9**, 395 (2019).

42. Rooney, A. D. et al. Calibrating the coevolution of Ediacaran life and environment. *Proc. Natl Acad. Sci.* **117**, 16824–16830 (2020).

43. Evans, S. D., Diamond, C. W., Droser, M. L. & Lyons, T. W. Dynamic oxygen and coupled biological and ecological innovation during the second wave of the Ediacara Biota. *Emerg. Top. Life Sci.* **2**, 223–233 (2018).

44. Zhang, F. et al. Global marine redox changes drove the rise and fall of the Ediacara biota. *Geobiology* **17**, 594–610 (2019).

45. Li, Z. et al. Transient and stepwise ocean oxygenation during the late Ediacaran Shuram Excursion: insights from carbonate $\delta^{238}U$ of northwestern Mexico. *Precambrian Res.* **344**, 105741 (2020).

46. Wang, H. et al. Sulfate triple-oxygen-isotope evidence confirming oceanic oxygenation 570 million years ago. *Nat. Commun.* **14**, 4315 (2023).

47. Mills, D. B. & Canfield, D. E. Oxygen and animal evolution: did a rise of atmospheric oxygen "trigger" the origin of animals? *BioEssays* **36**, 1145–1155 (2014).

48. Sperling, E. A. et al. Statistical analysis of iron geochemical data suggests limited late Proterozoic oxygenation. *Nature* **523**, 451–454 (2015).

49. Zhang, F. et al. Extensive marine anoxia during the terminal Ediacaran Period. *Sci. Adv.* **4**, eaan8983 (2018).

50. Evans, S. D. et al. Environmental drivers of the first major animal extinction across the Ediacaran White Sea-Nama transition. *Proc. Natl Acad. Sci.* **119**, e2207475119 (2022).

51. Wood, R. A. et al. Dynamic redox conditions control late Ediacaran metazoan ecosystems in the Nama Group, Namibia. *Precambrian Res.* **261**, 252–271 (2015).

52. Urey, H. On the early chemical history of the Earth and the origin of life. *Proc. Natl Acad. Sci. USA* **38**, 351–363 (1952).

53. Bjerrum, C. J. & Canfield, D. E. Towards a quantitative understanding of the late Neoproterozoic carbon cycle. *Proc. Natl Acad. Sci. USA* **108**, 5542–5547 (2011).

54. Busch, J. F. et al. Global and local drivers of the Ediacaran Shuram carbon isotope excursion. *Earth Planet. Sci. Lett.* **579**, 117368 (2022).

55. Yamauchi, M. Terrestrial ion escape and relevant circulation in space. *Ann. Geophys.* **37**, 1197–1222 (2019).

56. Gunell, H. et al. Why an intrinsic magnetic field does not protect a planet against atmospheric escape. *Astron. Astrophys.* **614**, L3 (2018).

57. Jackman, C. H., Fleming, E. L., Vitt, F. M. & Considine, D. B. The influence of solar proton events on the ozone layer. *Adv. Space Res.* **24**, 625–630 (1999).

58. Nicolet, M. On the photodissociation of water vapour in the mesosphere. *Planet. Space Sci.* **32**, 871–880 (1984).

59. Roberts, A., Pike, C. R. & Verosub, K. L. Forc diagrams: a new tool for characterizing the magnetic properties of natural samples. *J. Geophys. Res.* **105**, 461 (2000).

60. Harrison, R. J. & Feinberg, J. M. FORCinel: an improved algorithm for calculating first-order reversal curve distributions using locally

weighted regression smoothing. *Geochem. Geophys. Geosyst.* **9**, 11 (2008).

61. Egli, R. VARIFORC: an optimized protocol for calculating non-regular first-order reversal curve (FORC) diagrams. *Glob. Planet. Change* **110**, 302–320 (2013).

62. Tarduno, J. A. et al. Paleomagnetism indicates that primary magnetite in zircon records a strong Hadean geodynamo. *Proc. Natl Acad. Sci.* **117**, 2309–2318 (2020).

63. O'Brien, T. et al. Arrival and magnetization of carbonaceous chondrites in the asteroid belt before 4562 million years ago. *Commun. Earth Environ.* **1**, 54–54 (2020).

64. Veitch, R. J. An investigation of the intensity of the geomagnetic field during Roman times using magnetically anisotropic bricks and tiles. *Arch. Sci. Geneve.* **37**, 359–373 (1984).

65. Zhuravlev, A. Y. & Wood, R. A. The two phases of the Cambrian Explosion. *Sci. Rep.* **8**, 16656 (2018).

66. Darroch, S. A. F., Smith, E. F., Laflamme, M. & Erwin, D. H. Ediacaran Extinction and Cambrian explosion. *Trends Ecol. Evol.* **33**, 653–663 (2018).

67. Muscente, A. D., Boag, T. H., Bykova, N. & Schiffbauer, J. D. Environmental disturbance, resource availability, and biologic turnover at the dawn of animal life. *Earth Sci. Rev.* **177**, 248–264 (2018).

## Author contributions
W.H. collected paleointensity, rock magnetic and electron microscope data, analyzed the results, contributed to implications for the dynamo, ICN and animal radiations, and wrote the manuscript with contributions from all authors. J.A.T. conceived the study as part of a larger project with A.V.S., K.P.K. and M.I.M., conducted field work in South Africa, analyzed paleointensity data and rock magnetic data, contributed consideration of paleointensity history and ICN, magnetic shielding, atmospheric loss and potential linkages to animal radiation, and wrote the manuscript with contributions from all the authors. T.Z. contributed electron microscope analyses and to considerations of paleointensity history. M.I.M. contributed to the geochronologic and geological interpretations and overall project design. L.D.B. conducted field studies in South America, collected samples and provided geologic context including geochronology. E.K. provided geologic context including geochronology for samples from South America. E.G.B. contributed theoretical consideration on magnetic shielding and atmospheric loss. A.V.S. contributed magnetic susceptibility data and to overall project development. G.A. contributed magnetic susceptibility data. R.D.C. analyzed paleointensity and rock magnetic data. K.P.K. contributed to the overall project development, paleointensity history, and ICN. R.K.B. contributed to paleointensity history, field stability, ICN and data analysis. Y.-X.L. contributed to paleointensity history, field stability and ICN. F.N. contributed to the consideration of implications for the dynamo and ICN. S.X. provided paleobiology/paleoenvironment context. M.K.W. conducted field work in South African and contributed geologic interpretations.

## Competing interests
The authors declare no competing interests. Field work and sample collection was conducted with or by individuals associated with institutions in South Africa or Brazil with appropriate permissions for geological sampling. Specifically, field work in South Africa was conducted by J.A.T. and M.K.W. Field work in South America was conducted by L.D.B.

## Additional information
**Supplementary information** The online version contains supplementary material available at https://doi.org/10.1038/s43247-024-01360-4.

**Correspondence** and requests for materials should be addressed to John A. Tarduno.

**Peer review information** *Communications Earth & Environment* thanks Joseph Meert and the other, anonymous, reviewer(s) for their contribution to the peer review of this work. Primary Handling Editor: Carolina Ortiz Guerrero. A peer review file is available.

**Reprints and permissions information** is available at http://www.nature.com/reprints

**Publisher's note** Springer Nature remains neutral with regard to jurisdictional claims in published maps and institutional affiliations.